

1 Off-target *In Vitro* Profiling Demonstrates that Remdesivir Is a Highly Selective Antiviral Agent

2

3 Yili Xu, Ona Barauskas*, Cynthia Kim, Darius Babusis, Eisuke Murakami, Dmytro Kornyejev,

4 Gary Lee, George Stepan, Michel Perron*, Roy Bannister, Brian E. Schultz, Roman Sakowicz,

5 Danielle Porter, Tomas Cihlar, Joy Y. Feng#

6

7 Gilead Sciences, Inc., Foster City, CA 94404, USA

8

9 Running title: In vitro toxicity evaluation of remdesivir

10

11 #Address correspondence to Joy Y. Feng, joy.feng@gilead.com

12

13 *Present address: Ona Barauskas, Vir Biotechnology San Francisco, California; Michel Perron,
14 Janssen BioPharma Inc., Janssen Pharmaceutical Companies, South San Francisco, California.

15

16 **Abstract**

17 Remdesivir (RDV, GS-5734), the first FDA-approved antiviral for the treatment of COVID-19,
18 is a single diastereomer monophosphoramidate prodrug of an adenosine analogue. It is
19 intracellularly metabolized into the active triphosphate form, which in turn acts as a potent and
20 selective inhibitor of multiple viral RNA polymerases. RDV has broad-spectrum activity against
21 members of the coronavirus family such as SARS-CoV-2, SARS-CoV, and MERS-CoV, as well
22 as filoviruses and paramyxoviruses. To assess potential for off-target toxicity, RDV was
23 evaluated in a set of cellular and biochemical assays. Cytotoxicity was evaluated in a set of
24 relevant human cell lines and primary cells. In addition, RDV was evaluated for mitochondrial
25 toxicity under aerobic and anaerobic metabolic conditions, and for the effects on mitochondrial
26 DNA content, mitochondrial protein synthesis, cellular respiration, and induction of reactive
27 oxygen species. Lastly, the active 5'-triphosphate metabolite of RDV, GS-443902, was evaluated
28 for potential interaction with human DNA and RNA polymerases. Among all of the human cells
29 tested under 5-14 days of continuous exposure, RDV's CC_{50} values ranged from 1.7 to $>20 \mu\text{M}$,
30 resulting in selectivity indices (SI, CC_{50}/EC_{50}) from >170 to 20,000, with respect to RDV anti-
31 SARS-CoV-2 activity (EC_{50} of 9.9 nM in human airway epithelial cells). Overall, the cellular
32 and biochemical assays demonstrated a low potential of RDV for off-target toxicity including
33 mitochondria-specific toxicity, consistent with the reported clinical safety profile.

34

35 Introduction

36 Nucleoside/tide analogs have played a key role in the treatment of viral infections caused
37 by DNA viruses such as herpes virus and hepatitis B virus as well as RNA viruses such as human
38 immunodeficiency virus (HIV) and hepatitis C virus (HCV) (1, 2). Studies over the past several
39 decades have significantly expanded our knowledge on the potential off-target effects for this
40 class of compounds including inhibition of host nucleic acid polymerases such as human
41 mitochondrial DNA polymerase γ (POL γ) (3) and mitochondrial RNA polymerase (POLRMT)
42 (4, 5) as well as perturbation of nucleotide metabolism, mitochondrial respiration, and
43 dNTP/NTP pools (6). Importantly, suitable methods to evaluate the potential for these types of
44 toxicities are currently available.

45 Remdesivir (RDV, GS-5734) is a single diastereomer monophosphoramidate prodrug of
46 an adenosine analog (Fig. 1). Remdesivir has broad-spectrum activity against coronaviruses
47 (SARS-CoV-2, SARS-CoV, and MERS-CoV) (7, 8), filoviruses (Ebola virus [EBOV] and
48 Marburg virus) (9, 10), and paramyxoviruses (respiratory syncytial virus [RSV], Nipah virus,
49 and Hendra virus) (11, 12). RDV the first FDA-approved antiviral for the treatment of COVID-
50 19. . Its safety has been evaluated in two Phase I studies in healthy volunteers (13) and multiple
51 Phase III studies in Ebola-infected (14) and SARS-CoV-2-infected patients (15-17). These
52 studies demonstrated RDV as an effective antiviral agent with a favorable benefit/risk profile and
53 RDV addresses a serious unmet medical need to the treatment of patients with COVID-19. It is
54 intracellularly metabolized to its active triphosphate form (GS-443902, Fig. 1), which in turn acts
55 as a potent and selective inhibitor of multiple viral RNA polymerases. Additional metabolites are
56 formed both intracellularly and systemically in plasma including alanine metabolite (GS-
57 704277), parent nucleoside (GS-441524), and mono- and di-phosphate metabolites. To assess the

58 potential off-target toxicity of RDV, the drug and its metabolites including parent nucleoside
59 analog (GS-441524), intermediate metabolite MetX (GS-704277), and active triphosphate
60 metabolite (GS-443902) (Fig. 1) were characterized in a broad panel of cellular and biochemical
61 assays.

62 **RESULTS**

63 **Evaluation of cytotoxicity**

64 *Cytotoxicity in human cell lines and primary cells.* The cytotoxicity of RDV and GS-441524 was
65 tested in four immortalized human cell lines (laryngeal, hepatoma, prostate, and lymphoblastoid
66 transformed cell lines) and in seven primary human cell types including primary human
67 hepatocytes (PHH), primary renal proximal tubule epithelial cells (RPTECs), quiescent and
68 stimulated human peripheral blood mononuclear cells (PBMCs), and human hematopoietic
69 progenitor cells including erythroid, myeloid, and megakaryoid progenitors (Table 1). These
70 cells were chosen for their reported high sensitivity to or potential organ toxicity associated with
71 nucleoside/tide analogs (6). ATP level was used as an indication of cell viability. After 5-14 days
72 of continuous exposure to RDV, the CC_{50} values ranged from 1.7 to $> 20 \mu\text{M}$, resulting in
73 selectivity indices (SI, CC_{50}/EC_{50}) from >170 to 20,000, with respect to RDV anti-SARS-CoV-2
74 activity (EC_{50} of 9.9 nM in human airway epithelial cells [HAE]) (18). Among the four cell lines
75 tested, the MT-4 cell line was the most sensitive towards RDV and GS-441524, consistent with
76 reports using other nucleoside/tide analogues (5, 19). Among the seven primary cell types tested,
77 PHH showed the lowest CC_{50} towards RDV, suggesting that PHHs are susceptible to RDV-
78 mediated toxicity.

79 The parent nucleoside GS-441524 showed no cytotoxicity up to $100 \mu\text{M}$ in any of the cell
80 lines tested, except in MT-4 ($CC_{50} = 69 \pm 26 \mu\text{M}$). Among the primary human cells, GS-441524

81 showed no toxicity at the highest concentration tested (100 μM), except in the three human
82 hematopoietic progenitor cells ($\text{CC}_{50} = 9.6\text{-}13.9 \mu\text{M}$ after 11-14 days of exposure).

83 *Effect on production of reactive oxygen species.* Reactive oxygen species (ROS) including
84 peroxides, superoxides, and hydroxyl radicals are natural byproducts of normal cell metabolism
85 and have important roles in cell signaling and homeostasis. However, excessive production of
86 ROS can be induced by drugs and may result in cellular damage and cell death (20). In this
87 study, we evaluated the potential effects of RDV on ROS generation in HepG2 cells, a human
88 hepatic cell line. After a 24-hour incubation, RDV-treated cells showed no significant increase in
89 ROS levels at concentrations up to 50 μM , and a 60% increase at 100 μM ($p = 0.042$ compared
90 with DMSO control) accompanied by a parallel 60% decrease in cell viability, indicating that
91 ROS is unlikely to be the driver of cytotoxicity (Figure 2). In comparison, the control compound
92 menadione showed > 3-fold increase in ROS levels after a 30-minute incubation.

93 **Evaluation of mitochondrial toxicity**

94 *Cytotoxicity under aerobic metabolic conditions.* Some nucleoside analogues have the potential
95 to affect mitochondrial functions via diverse mechanisms. One approach to assess mitochondrial
96 function is a comparison of effects on cell viability in the presence of glucose-favoring
97 glycolysis (ie, anaerobic metabolism) and galactose-favoring oxidative phosphorylation
98 (ie, aerobic metabolism). The latter condition may sensitize cells to compounds affecting
99 mitochondrial functions (21). However, the predictability of this assay has not been validated for
100 nucleoside/tide analogues (6). Using intracellular ATP quantification as a readout for cell
101 viability, the effects of glucose and galactose on the cytotoxicity of RDV and GS-441524 were
102 assessed in the HepG2 hepatoma cell line, which was previously identified as a suitable model
103 for testing compounds under aerobic conditions (Table 2) (21). In addition, a similar study was

104 done using the PC-3 prostate-derived cell line, a model of rapidly proliferating cells. The CC_{50}
105 values of RDV in HepG2 cells were 3.7 and 11.1 μM in the presence of glucose and galactose,
106 respectively (Table 2), indicating that aerobic conditions did not enhance the cytotoxicity of
107 RDV. In contrast, aerobic conditions in PC-3 cells enhanced RDV cytotoxicity by 6-fold
108 ($CC_{50} = 1.4$ in galactose culture vs 8.9 μM in glucose culture). The divergent results from HepG2
109 and PC-3 cells suggest that the observed effects are cell line-dependent.

110 The parent nucleoside GS-441524 did not show any cytotoxicity in either PC-3 or HepG2
111 cells at the highest concentrations tested (100 μM), irrespective of the metabolic conditions
112 (Table 2). Puromycin, used as general cytotoxic control, exhibited similar cytotoxicity in both
113 cell types in the presence of glucose or galactose. The lack of a known nucleoside mitotoxin
114 prevented us from using one as a positive control in this study.

115 *Effect on mitochondrial DNA.* The potential effect of RDV and GS-441524 on mitochondrial
116 DNA (mtDNA) was assessed in vitro by quantitative real-time polymerase chain reaction
117 (qPCR) analysis following continual treatment of HepG2 cells for 10 days. Dideoxycytidine
118 (ddC), a known inhibitor of mtDNA replication, was used as a positive control. HepG2 cells
119 treated with RDV showed a lack of dose response indicating the lack of a specific effect on
120 mtDNA synthesis. The effect of the parent nucleoside GS-441524 on mtDNA content was
121 overall minimal (Table S1).

122 *Effect on mitochondrial protein synthesis.* The effect of RDV and GS-441524 on mitochondrial
123 protein synthesis was assessed following a 5-day incubation with PC-3 cells. This particular cell
124 model was chosen for its prior successful use in the studies of mitochondrial toxins (6). The
125 selective effect of a compound on mitochondrial protein synthesis was determined by
126 quantification of the level of cytochrome oxidase subunit 1 (COX-1; encoded by mtDNA) and

127 succinate dehydrogenase A (SDH-A; encoded by nuclear DNA) (5, 19). RDV affected the levels
128 of COX-1 and SDH-A to a similar extent, with CC_{50} values of 8.9 and 8.6 μM , respectively
129 (Table 3, Figure 3). These effects manifested in the same range of concentrations as the
130 cytotoxicity measured by cellular ATP levels, indicating a lack of any selective effect of RDV on
131 mitochondrial protein synthesis. GS-441524 showed no effect on protein synthesis up to the
132 highest concentration tested (100 μM) (Table 3, Figure 3). Chloramphenicol was used as a
133 positive control, and its specific effect on mitochondrial protein synthesis was consistent with
134 published data (5, 19).

135 *Effect on mitochondrial respiration.* RDV and GS-441524 were further evaluated for their
136 effects on mitochondrial spare respiratory capacity in the human cell-lines PC-3 and HepG2 and
137 the primary cells PHH and RPTEC by measuring the rate of oxygen consumption (OCR) using a
138 Seahorse Extracellular Flux Analyzer (5, 22-24). Overall, there was a lack of a specific effect on
139 cellular respiration among the four cellular systems tested. The cellular respiration of RDV-treated
140 cells decreased in parallel with decreases in ATP level and total DNA level in HepG2, PHH, and
141 RPTEC, indicating a lack of specific inhibition of cellular respiration (Table 4, Figure 4). The
142 most profound effect of RDV on spare mitochondrial respiratory capacity was seen in PC-3 cells,
143 where RDV inhibited mitochondrial spare respiratory capacity with a
144 CC_{50} value ($CC_{50} = 2.5 \mu\text{M}$) lower than those for the inhibition of ATP level and total DNA
145 ($CC_{50} = 24.0$ and $12.5 \mu\text{M}$, respectively). Among all four cell systems, GS-441524 showed no
146 effect on mitochondrial respiration at the highest concentration tested (100 μM) (Table 4, Figure
147 S1). In contrast, the positive control chloramphenicol showed specific inhibition of
148 mitochondrial respiration and minimal impact on ATP level and total DNA (Figure S2).

149 GS-704277, a major intermediate RDV metabolite was evaluated for its effect on
150 mitochondrial spare respiratory capacity, ATP levels, and total DNA in PHH after both an acute
151 4-hour treatment and a chronic 3-day incubation, the default condition in the experiments
152 described in the previous paragraph. After the 4-hour incubation, RDV-treated PHH showed
153 parallel decreases in mitochondrial spare respiratory capacity (21%-27%) and cellular ATP
154 levels (17%-31%), indicating lack of mitochondria-specific toxicity (Figure S3). After a 3-day
155 treatment with RDV, PHH showed parallel decreases in mitochondrial spare respiratory capacity,
156 ATP levels, and total DNA, with CC_{50} values of 7.6, 7.8, and 13.4 μM , respectively, indicating
157 general toxicity instead of specific mitochondrial toxicity (Table 4, Figure 4). Neither of the
158 two major systemic metabolites of RDV, GS-704277 nor GS-441524, exhibited any effects on
159 mitochondrial spare respiratory capacity, ATP levels, or total DNA at the highest concentration
160 tested (100 μM) after either a 4-hour or a 3-day treatment (Table 4, Figure S1, S3-S4).

161 **Profiling of the active triphosphate metabolites**

162 *Formation of active 5'-triphosphate metabolite GS-443902 in cells*

163 Formation of GS-443902 from RDV and GS-441524 was measured in HEp-2, PC-3, and PHH
164 cells after 24-hour continuous incubation of the compounds. As shown in Figure 5 and Table S2,
165 RDV formed 43 ± 6 , 153 ± 16 , and 45 ± 23 pmole/ 10^6 cells of GS-443902 in HEp-2, PC-3, and
166 PHH cells, respectively. In contrast, GS-441524 formed 7.8-23-fold less active metabolites in
167 these cells, at 5.5 ± 1.1 , 6.6 ± 4.9 and 1.9 ± 1.6 pmole/ 10^6 cells, respectively.

168 *Interaction with host RNA and DNA polymerases.* The active triphosphate metabolite GS-443902
169 was tested in multiple biochemical assays to assess its interaction with key human DNA and
170 RNA polymerases. The enzymatic activities of human DNA polymerases α and β , as well as that
171 of RNA polymerase II, were unaffected by GS-443902 up to 200 μM , the highest concentration

172 tested (Table 5). In addition, GS-443902 was tested for its incorporation into nucleic acids by
173 host mitochondrial DNA and RNA polymerases using a single nucleotide incorporation assay.
174 GS-443902 was a poor substrate of mtDNA polymerase γ with no detectable incorporation when
175 tested under the supratherapeutic concentration of 50 μM [vs C_{max} of 6 μM at 150 mg dose in
176 clinic (13). It was also a poor substrate for POLRMT, with a rate of incorporation equal to 5.8%
177 relative to ATP when tested under supratherapeutic concentration of 500 μM (Table 6). This
178 result contrasts with the significantly higher incorporation rates of 92% and 112%, for the
179 triphosphate forms of BMS-986094 and balapiravir, respectively, two anti-HCV nucleosides
180 associated with clinical toxicity (5). Together, these data further support the hypothesis about
181 low potential of RDV to induce mitochondrial toxicity.

182 **Molecular target screen**

183 In addition to the aforementioned known off-targets of nucleoside/tide analogues, the RDV-
184 containing diastereomeric mixture GS-466547 and the parent nucleoside GS-441524 were
185 screened against a panel of 87 targets consisting of receptors, ion channels, transporters, and
186 enzymes involved in a wide range of biological processes (Table S3). At 10 μM , none of the
187 compounds showed detectable interaction with any of the 87 targets tested.

188 **DISCUSSION**

189 RDV is a single diastereomer monophosphoramidate prodrug of an adenosine analog
190 with broad-spectrum antiviral activity. Using a prodrug as a way to deliver an active molecule
191 may potentially result in intracellular accumulation of the less cell-permeable metabolites
192 depending on the activity of the enzymes participating in the metabolism of a particular drug and
193 its conversion into the active form. Therefore, detailed examination of the functional
194 consequences of the exposure to high doses is critical for the evaluation of the drug safety.

195 This study presents a detailed characterization of RDV in a panel of in vitro cytotoxicity
196 and off-target screening assays, undertaken to identify potential safety and toxicity liabilities. In
197 this report, the general cytotoxicity of RDV measured as CC_{50} following a 5- to 14-days of
198 continuous exposure to the drug ranged from 1.7 μM to $>20 \mu\text{M}$ in selected human cell lines and
199 primary human cells. It is worth noting that the RDV exposure in these cell culture studies was
200 significantly higher than the systemic exposure of RDV for the repeated dosing of 150 mg in
201 humans (plasma $C_{\text{max}} = 2720 \text{ ng/mL} = 4.5 \mu\text{M}$, $t_{1/2} = 1.11 \text{ hr}$) (13). The parent nucleoside and
202 major systemic metabolite GS-441524 showed less cytotoxicity than RDV. The differences in
203 toxicity between these two compounds are likely due to the significantly lower active
204 triphosphate in GS-441524-treated cells than in RDV-treated cells, as observed in this study as
205 well as other studies (18). However, RDV and GS-441524 showed similar levels of toxicity in
206 three hematopoietic progenitor cells. Cell-dependent cytotoxicity has been widely observed for
207 nucleoside/tide analogs, which can be affected by the duration of compound exposure (5-day
208 versus 14-day), compound permeability, intracellular activation, and differential cellular
209 characteristics including replication rate and bioenergetic status (5).

210 Among the primary cells tested, PHH showed the highest sensitivity to RDV, possibly
211 due to high cellular permeability and efficient intracellular metabolism leading to high levels of
212 the triphosphate metabolite. This observation could shed light on the liver enzyme elevations
213 observed in healthy volunteers treated with repeated doses of RDV (13). In contrast, the two
214 main RDV metabolites in plasma, GS-704277 and GS-441524, are unlikely to contribute to
215 clinical liver toxicity, due to their low permeability and ineffective intracellular metabolism or
216 limited systemic exposure. In two Phase I studies, RDV was evaluated in healthy subjects with
217 single-dose IV administration (across the dose range of 3-225 mg; N=78 RDV and 18 placebo)

218 or multiple doses of 150 mg once daily for 7 or 14 days (N=16 RDV and 8 placebo) (13).

219 Overall, RDV was well tolerated in both studies, and all adverse events were Grade 1 or 2 in

220 severity. In the repeat-dose study, reversible, treatment-emergent Grade 1 or 2 alanine

221 aminotransferase (ALT) (50% RDV, 13% placebo) and aspartate aminotransferase (AST) (44%

222 RDV, 0% placebo) elevations were observed . Because transaminase elevations have been

223 observed in patients with COVID-19 (25), the potential of RDV to exacerbate transaminase

224 elevations in patients with COVID-19 may be difficult to discern. This has been supported by

225 multiple RDV clinical trials. First, an open-label study (N=397 RDV) without a placebo control

226 arm showed little difference between 5-day and 10-day RDV treatment durations for adverse

227 events of elevations in ALT (6% and 8%, respectively) or AST (5% and 7%, respectively) (15).

228 Second, in a study of RDV in 584 hospitalized patients with moderate COVID-19, patients were

229 randomized at a 1:1:1 ratio to receive 10-day RDV, 5-day RDV, or standard of care treatment;

230 there was little difference between the three arms for adverse events of elevations in ALT (32%,

231 34%, and 39%, respectively) or AST (32%, 32%, and 33%, respectively); Grade 3 or 4 adverse

232 events were reported less frequently for patients who received RDV (ALT: 3%, 2%, and 8%,

233 respectively; AST: 1%, 3%, and 6%, respectively) (17). Finally, in the recently completed

234 double-blind study of RDV versus placebo in 1062 hospitalized patients with COVID-19,

235 adverse events of increased amino transferase levels, including ALT, AST, or both were reported

236 in 6% of subjects treated with RDV for up to 10 days compared with 11% of subjects in the

237 placebo group, indicating lack of specific drug-induced liver enzyme elevation (16). All of these

238 reports consistently support minimal contribution of RDV to transaminase elevations in patients

239 with COVID-19.

240 To understand whether the cytotoxicity is associated with mitochondrial toxicity, we
241 measured the effects of RDV on mitochondrial DNA content, protein level, and cellular
242 respiration. In HepG2 cells, RDV showed a lack of a specific dose-dependent effect on mtDNA
243 synthesis. Similarly, RDV did not show specific inhibition of a mitochondria DNA-coded protein
244 (CC₅₀ of 8.9 μ M) over a nuclear DNA-coded protein (CC₅₀ of 8.6 μ M) in PC-3 cells. Additional
245 biochemical assays showed that the active triphosphate metabolite GS-443902 was a poor
246 substrate for mitochondria DNA and RNA polymerases even when tested at supra-physiological
247 concentrations of 50 and 500 μ M, respectively. A recent paper reported the effects of RDV on
248 cellular toxicity through a transcriptomic analysis, and reported effects of RDV on mitochondrial
249 function (31). However, it is not clear whether the results were due to specific mitochondrial
250 toxicity or general cellular toxicity. In addition, the relation between specific gene expression
251 and mitochondrial toxicity has not been fully validated.

252 Taken together, we conclude that RDV has low potential for the off-target toxicities
253 described for other nucleoside analogs including mitochondrial toxicity. Furthermore, neither
254 RDV nor its systemic metabolites induced ROS formation *in vitro* or interacted with any of the
255 87 targets in the molecular screen. Consistent with the clinical observations of drug-related
256 elevations of liver transaminases following multiple doses of RDV, primary hepatocytes showed
257 high *in vitro* susceptibility to RDV. In clinical settings of COVID-19 treatment in hospitalized
258 patients, the risk associated with possible RDV-related liver enzyme elevations is substantially
259 lower compared to its established benefits in hospitalized COVID-19 patients.

260 MATERIALS AND METHODS

261 **Reagents.** Remdesivir (RDV, GS-5734), its parent nucleoside GS-441524, metabolite
262 intermediate GS-704277 (Met X), and 5'-triphosphorylated metabolite GS-443902 were

263 synthesized by Gilead Sciences, Inc (Foster City, CA). Nucleotide triphosphates (TP) used as
264 positive controls including decitabine-TP (5-aza-2'-deoxyCTP), 2'CMe-GTP (active metabolite
265 of BMS-986094), 4'-CN-CTP (active metabolite of Balapiravir/RG1626) were synthesized by
266 Gilead Sciences, Inc. 3'-deoxy ATP, 3'-deoxy GTP, 3'-deoxy CTP, 3'-deoxy UTP were
267 purchased from TriLink BioTechnologies (San Diego, CA). Control compounds for CC₅₀ assays
268 such as dideoxycytidine (ddC), puromycin, chloramphenicol, menadione, aphidicolin, and α -
269 amanitin were purchased from Sigma-Aldrich (St. Louis, MO). All radioactively labeled
270 nucleoside triphosphates (NTPs) were purchased from PerkinElmer (Shelton, CT).

271 **Cell lines and primary cells.** The following cell lines were obtained from the indicated sources:
272 HEp-2 (laryngeal carcinoma; ATCC), HepG2 (hepatoblastoma; ATCC), PC-3 (prostate
273 metastatic carcinoma; ATCC), and MT-4 [human T-cell leukemia virus 1 (HTLV-1)-transformed
274 human T lymphoblastoid cells; NIH AIDS Research and Reference Reagent Program].
275 Cryopreserved primary human RPTEC were obtained from LifeLine Cell Technology
276 (Frederick, MD) and isolated from the tissue of human kidney. Freshly isolated PHH were from
277 Bioreclamation IVT (Westbury, NY) or Life Technologies (Carlsbad, CA). Human PBMC were
278 isolated from human buffy coats which were obtained from healthy volunteers (Stanford Blood
279 Bank, Palo Alto, CA).

280 **Cell culture.** The HepG2 galactose-adapted cell line was established by culturing HepG2 cells in
281 glucose-free DMEM (Gibco, Carlsbad, CA) supplemented with 10% FBS, 100 units/mL
282 penicillin, 100 units/mL streptomycin, 2 mM glutamine, 1 mM sodium pyruvate, and 10 mM
283 galactose for 3 weeks prior using in the assays. The PC-3 galactose-adapted cell line was
284 established by culturing PC-3 cells in glucose-free Kaighn's F12 media supplemented with 10%
285 FBS, 100 units/mL penicillin, 100 units/mL streptomycin, and 7 mM galactose for 3 weeks prior

286 using in the assays. The cells were passaged twice per week to maintain sub-confluent densities.
287 The cell culture procedures of RPTEC and PHH were following vendor's recommendation.
288 PBMCs were isolated from human buffy coats using standard Ficoll separation and stimulated as
289 described elsewhere (19) and were tested at both quiescent and stimulated stages. The stimulated
290 PBMCs were obtained from quiescent PBMCs stimulated with 10 units per mL of recombinant
291 human interleukin 2 (hIL-2) and 1 μ g per mL phytohemagglutinin P (PHA-P) for 48 hrs prior to
292 drug treatment. Normal human primary bone marrow (BM) light-density cells were from three
293 different lots obtained from AllCells (Emeryville, CA) or Lonza (Walkersville, MD). All
294 primary human cells were cultured according to the manufacturer's protocols. All cells were
295 cultured at 37 °C in a 5% CO₂ incubator with 90% humidity unless noted otherwise.

296 **General cytotoxicity and cell viability.**

297 *Cytotoxicity in human cell-lines, PHH, RPTEC, and PBMC.* Cells were treated with compounds
298 for 4 hours to 14 days depending on assay type. Culture of freshly isolated PHH cells required
299 fresh medium every 24-48 hours so compounds and medium were refreshed on Day 0, 2, and 4
300 or Day 0, 1, 3 during the 5-day culture. After the incubation period, cell viability was measured
301 by the addition of CellTiter Glo viability reagents (Promega, Madison, WI). The luminescence
302 signal was quantified on an EnVision or VictorTM luminescence plate reader (Perkin-Elmer,
303 Waltham, MA) after the cells were incubated with the reagents for 10 min at room temperature.
304 The compound concentration that caused a 50% decrease in the luminescence signal (CC₅₀), a
305 measure of toxicity, was calculated by nonlinear regression using a sigmoidal dose-response
306 (variable slope) equation as described in Data Analysis Section.

307 *Cytotoxicity in human hematopoietic progenitor cells.* The effects of the compounds on the
308 proliferation of human erythroid, myeloid, and megakaryoid progenitors were tested in

309 MethoCult84434, a methylcellulose-based colony assay conducted by StemCell Technology
310 (Vancouver, Canada) (26). After 11-14-day culture, the hematopoietic progenitor colonies
311 (CFU-E, BFU-E, CFU-GM, and CFU-GEMM [E, erythroid; BFU, burstforming unit; GM,
312 granulocyte/macrophage; GEMM, multilineage progenitors]) were enumerated and the CC_{50}
313 values were calculated as described in Data Analysis section.

314 **Detection of intracellular reactive oxygen species (ROS) level.** HepG2 cells were seeded at
315 densities of 12×10^3 cells per well in 96-well plates with a final volume of 160 μ L per well. The
316 cells were incubated overnight at 37 °C in a 5% CO₂ and 90% humidity incubator with EMEM
317 medium supplemented with 10% FBS (HyClone, Logan, UT), 100 units/mL penicillin and 100
318 μ g/mL streptomycin (P/S) (Gibco, Carlsbad, CA). On the next day (Day 1), cells in 42 out of the
319 96-well plate were treated with RDV for 24 hours. RDV was added to the cell culture plate
320 directly using an HP D300 Dispenser (Hewlett-Packard, Palo Alto, CA) with a starting
321 concentration of 100 μ M, with two-fold dilutions to generate a total of 6 concentration points
322 with six replicates for each concentration and 6 wells without RDV as negative controls. On the
323 day of the ROS assay (Day 2), 18 wells out of the remaining untreated 54 wells on the original 96-
324 well plate were incubated with either 0 μ M, 100 μ M, or 200 μ M menadione (Sigma-Aldrich, St.
325 Louis, MO) for 30 minutes, with 6 replicates for each treatment. A mixture of CellROX Deep
326 Red reagent and NucBlue Hoechst 33342 was added to the cells treated with menadione, RDV,
327 and DMSO. The final DMSO concentration was 0.5% in all wells. The cell culture plate was
328 incubated in a 37 °C incubator for 30 minutes. The cell culture plate was then washed 3-4 times
329 with 200 μ L/well of 1 \times PBS buffer without Ca²⁺ and Mg²⁺ (Corning, Corning, New York),
330 followed by a final addition of 100 μ L 1 \times PBS in each well. The assay plate was scanned using a
331 CellomicsTM ARRAYSCAN VTI (Thermo Fisher Scientific, Waltham, MA) High Content

332 Screening Instrument with two channels. One channel measured the intensity of CellROX Deep
333 Red using excitation/emission at 640/665 nm, while the other channel measured the signal
334 intensity from NucBlue/Hoechst 3334 using excitation/emission at 360/460 nm. The ATP level
335 was measured using CellTiter Glo viability reagents (Promega, Madison, WI) in cells treated
336 with RDV for 24 hours in a parallel experiment.

337 **Data analysis.**

338 *Data analysis of Calculation of CC₅₀ and IC₅₀ values.* The CC₅₀ values were defined as the
339 concentration causing 50% decrease in cell viability, DNA level, protein level, or spare
340 respiratory capacity in comparison to the DMSO control. The IC₅₀ values were defined as the
341 concentration causing 50% decrease in product formation in the biochemical assays. Data were
342 analyzed using GraphPad Prism 8.0 (La Jolla, CA). The CC₅₀ and IC₅₀ values were calculated by
343 non-linear regression analysis using sigmoidal dose-response (variable slope) equation (four
344 parameters logistic equation):

$$345 Y = 100 / (1 + 10^{((\text{LogCC}_{50} - X) * \text{Hillslope}))})$$

$$346 Y = 100 / (1 + 10^{((\text{LogIC}_{50} - X) * \text{Hillslope}))})$$

347 where X is the log of the concentration of the test compound, Y is the response. The CC₅₀ or IC₅₀
348 values were calculated as an average of three or more independent experiments.

349 *Data analysis of measuring mitochondrial DNA.* The relative amount of mitochondrial DNA
350 (mtDNA) in treated samples was determined using a relative quantification method based upon
351 the $2^{-\Delta\Delta C_T}$ formula (27). The amount of mtDNA in compound treated samples relative to the
352 DMSO treated controls (% mtDNA) was calculated based upon the following formula:

$$353 \% \text{ mtDNA} = 100 \times 2^{-\Delta\Delta C_T}$$

$$354 \Delta\Delta C_T = \Delta C_{T, \text{ treated}} - \Delta C_{T, \text{ control}}$$

355 $\Delta C_{T, \text{treated}} = (C_{T, \text{cyt b}} - C_{T, \beta\text{-actin}})_{\text{treated}}$

356 $\Delta C_{T, \text{control}} = (C_{T, \text{cyt b}} - C_{T, \beta\text{-actin}})_{\text{control}}$

357 $C_{T, \text{cyt b}}$ and $C_{T, \beta\text{-actin}}$ represent the cycle threshold values for the amplification of cytochrome
358 b and $\beta\text{-actin}$, respectively, as determined by the computational analysis of amplification curves
359 using the ABI Prism software. The final results are presented as the mean % mtDNA \pm SD from
360 2 independent experiments, each performed in triplicate. The $2^{-\Delta\Delta C_T}$ method was validated for
361 cytochrome b and $\beta\text{-actin}$ genes by determining the ΔC_T values for amplification reactions
362 containing various amounts of total cellular DNA. Minimal differences were observed in the ΔC_T
363 values in samples containing 5 to 40 ng of total cellular DNA; indicating that neither the
364 amplification nor detection efficiencies of cytochrome b and $\beta\text{-actin}$ were affected by the amount
365 of DNA template within the dilution range relevant for the quantitative analysis performed
366 (Table S5).

367 **Measuring mitochondrial DNA.** mtDNA was generated by real-time PCR from total DNA
368 isolated from HepG2 cells using the QIAamp DNA Mini Kit (Qiagen, Valencia, CA) according
369 to the manufacturer's protocol. Real-time PCR reactions were performed using TaqMan
370 universal mastermix (Applied Biosystems, Foster City, CA) in an ABI Prism 7900HT Fast Real-
371 Time PCR System (Applied Biosystems). Quantification of mtDNA was achieved by
372 amplification of a fragment of the mitochondrial specific cytochrome b gene using the primers
373 and probe. The oligonucleotide sequence of the primer and probe was used as cytochrome b
374 forward CCTCCACCCTTACTACACAATCAA, cytochrome b reverse
375 GGTCTGGTGAGAATAGTGTTAATGTCA, and cytochrome b FAM-
376 ACGCCCTCGGCTTAC-BHQ1. Chromosomal DNA was quantified by the amplification of a
377 fragment of the $\beta\text{-actin}$ gene using a $\beta\text{-actin}$ Assay-on-Demand kit (Applied Biosystems).

378 Amplification reactions for the quantification of mitochondrial and chromosomal DNA were
379 performed independently using approximately. HepG2 cell culture and compounds' treatment
380 was based on a previously published method (19, 28).

381 **Mitochondrial protein synthesis assay.** PC-3 cells were treated with the compounds for 5 days
382 and analyzed with the MitoTox MitoBiogenesis in-cell enzyme-linked immunosorbent assay
383 (ELISA) kit (MitoSciences/Abcam, Eugene, Oregon) as described previously (5, 19). The assay
384 uses quantitative immunocytochemistry to measure the protein levels of nuclear DNA-encoded
385 succinate dehydrogenase (SDH-A; Complex II) and mitochondrial DNA-encoded cytochrome c
386 oxidase (COX-1; Complex IV) in cultured cells.

387 **Mitochondrial respiration in cell lines and primary cells.** Mitochondrial respiration was
388 monitored by measuring the rate of oxygen consumption (OCR) of the cells after 4-hour or 3-day
389 treatments with the compounds, using a Seahorse extracellular flux analyzer (XFe-96) based on
390 published protocols (5, 22-24) and modified from a previously published method (5). The OCR
391 signals were normalized by cell numbers using DNA content which method was based on a
392 previously published method (5). The optimized cell seeding of PC-3, HepG2, RPTEC, and PHH
393 were seeded at densities of 5×10^3 , 5×10^3 , 7.5×10^3 , and 25×10^3 cells per well, respectively,
394 in XF 96-well plates (Seahorse Bioscience, North Billerica, MA) with a final volume of 160 μ L
395 per well. The cells were incubated with compounds for 3 days except PHH which received
396 compound treatment for 4 hours or 3 days. Compounds were added to the assay plate directly
397 using an HP D300 Dispenser (Hewlett-Packard, Palo Alto, CA) with 2-fold dilutions to give a
398 total of 9 concentration points with six replicates. On the day of the assay, the cell culture
399 medium was replaced with XF assay medium (pH 7.4) containing 10 mM glucose and 1 mM
400 freshly prepared pyruvate. The mitochondrial respiration was monitored by measuring the rate of

401 oxygen consumption (OCR) on a Seahorse Extracellular Flux (XFe-96) Analyzer based on
402 published protocols (5, 22-24). All concentrations were final after mixing unless noted
403 otherwise. Multiple parameters were measured after the sequential injection of the ATP synthase
404 inhibitor oligomycin (2 μ M for all cell models), the uncoupler FCCP (0.25 μ M for PC-3, 0.5 μ M
405 for HepG2 and PHH, 1.5 μ M for RPTEC), and a mixture of the mitochondrial Complex I
406 inhibitor rotenone and the Complex III inhibitor antimycin A (0.5 μ M of each for all cell models)
407 (Mito Stress Test Kit, Seahorse Biosciences) (22-24). The spare respiratory capacity was
408 obtained by subtracting the rate of basal respiration from the rate of maximal respiration and
409 normalized to the cell number obtained from DNA level measurements. The data reported for
410 each treatment are the average of the results from six replicates. The methods of detection of
411 measuring ATP level in parallel experiments was based on a previously published method (5).

412 **Biochemical assays.**

413 *DNA and RNA templates and primers.* The DNA polymerase alpha and gamma inhibition assays
414 utilized a 78-mer DNA template and a 19-mer DNA primer: D78 5'-
415 ACACATGATACTACGAATTTTATGCTTCCAATGCCTTACAGTTCTCTAGCGGTGGCG
416 CCCGAACA GGGACCTGAAAGC-3' and D19 5'-GTCCCTGTTCGGGCGCCAC-3' were
417 purchased from Integrated DNA Technologies (Coralville, IA). Activated fish sperm DNA was
418 purchased from USB/Affymetrix (Santa Clara, CA) and used as a template for the DNA
419 polymerase beta inhibition assay. The DNA template used in the RNA POLII inhibition assay
420 was a 1,188 bp restriction fragment containing the cytomegalovirus (CMV) immediate early
421 promoter (Promega, Madison, WI). For single nucleotide incorporation, a DNA 19-mer primer
422 and a DNA 36-mer template were used for POL γ -catalyzed reactions whereas a RNA 12-mer
423 primer and a DNA 18-mer template were used for POLRMT-catalyzed reactions (Table S6). All

424 primers were 5'-labeled with ^{32}P - γ -ATP (3000 Ci/mmol) and T4-kinase (New England Biolabs,
425 Ipswich, MA). In brief, a mixture containing 100 μM of primer, 0.4 unit/ μL T4-kinase, $1\times$ T4-
426 kinase reaction buffer, and 4 $\mu\text{Ci}/\mu\text{L}$ (0.4 μM) ^{32}P - γ -ATP was incubated at 37 $^{\circ}\text{C}$ for 60-120 min,
427 followed by heat-inactivation at 65 $^{\circ}\text{C}$ for 5-10 minute. 5'- ^{32}P -R12/D18 were annealed at a
428 1:1.1 molar ratio at a concentration of 10 μM in a solution of 10 mM Tris-HCl (pH 8.0) and 0.1
429 mM EDTA using a thermocycler where samples were heated for 1 minute at 90 $^{\circ}\text{C}$ and cooled to
430 10 $^{\circ}\text{C}$ at a rate of 5 $^{\circ}\text{C}$ per minute. 5'- ^{32}P -D18/D36 were annealed at a 1:1.1 molar ratio at 10 μM
431 in a solution containing 10 mM Tris-HCl (pH 8.0) and 0.1 mM EDTA. Samples were heated at
432 90 $^{\circ}\text{C}$ for 10 minutes, cooled at 50 $^{\circ}\text{C}$ for 30 minutes and placed on ice for 10 minutes.

433 *Enzymatic inhibition assays.* Human DNA polymerase alpha, isolated from HeLa cell extracts,
434 was from CHIMERx (Madison, WI). Recombinant human DNA polymerase beta, expressed in
435 *E. coli*, was a gift from Zucai Suo at The Ohio State University. Recombinant human DNA
436 polymerase gamma (including both the large subunit and the small subunit) was cloned,
437 expressed, and purified from insect cells by Gilead Sciences (Foster City, CA) (19). RNA PolIII
438 was purchased as part of the HeLaScribe nuclear extract in vitro transcription system kit from
439 Promega (Madison, WI). The recombinant human POLRMT and the transcription factors
440 mitochondrial transcription factor A (mtTFA) and B2 (mtTFB2) were purchased from Enzymax
441 (Lexington, KY). The inhibition of DNA polymerases alpha, beta, and gamma, POLRMT, and
442 PolII has been described previously in detail (4, 19, 29).

443 *Single nucleotide incorporation assay by human mitochondrial DNA Pol γ .* All concentrations
444 were given as the final concentration. 1.2 nM DNA Pol γ large subunit and 3.4 nM Pol γ
445 accessory subunit were preincubated on ice for 5 minutes and added to reaction mixture
446 containing 50 mM Tris-HCl (pH 8.0), 2 mM DTT, 0.2 mg/mL BSA, 200 nM D19/D36 p/t and 10

447 mM MgCl₂. Reactions were heated for 37 °C and initiated by addition of 50 μM natural dNTP or
448 analogs, plus 50 μM dGTP (for T or C template) or dCTP (for A or G template). At 0, 0.5, 2, 5,
449 10, 30, and 60 min, 10 μL of the reaction mixture was removed and quenched with 10 μL of gel
450 loading buffer containing 100 mM EDTA, 80% formamide, and 1% bromophenol blue, and
451 heated for 65 °C for 5 minutes. The samples were run on a 20% polyacrylamide gel (8 M urea)
452 and the gel was exposed to a phosphorimager screen. The substrate and the incorporation
453 products, D19 and D20-28, were quantified using a Typhoon Trio Imager and Image Quant TL
454 software.

455 *Single nucleotide incorporation assay by human mitochondrial POLRMT.* The assay was
456 modified based on a published report (30). All concentrations are final concentration. A mixture
457 of MTCN buffer (50 mM MES, 25 mM Tris-HCl, 25 mM CAPS, and 50 mM NaCl, pH 7.5), 200
458 nM 5'-³²P-R12/D18, 10 mM MgCl₂, 1 mM DTT, and 376 nM POLRMT (Enzymax, Lexington,
459 KY) was pre-inclubated at 30 °C for 1 min. The reaction was started by addition of 500 μM
460 natural NTP or NTP analogs. At 0.17, 0.5, 2, 5, 10, and 30 minutes, 3 μL of the reaction mixture
461 was removed and quenched with 10 μL of gel loading buffer containing 100 mM EDTA, 80%
462 formamide, and 1% bromophenol blue, and heated for 65 °C for 5 minutes. The samples were
463 run on a 20% polyacrylamide gel (8 M urea) and the gel was processed and analyzed in the same
464 way as described above.

465 **Molecular target screen of the RDV-containing diastereomeric mixture GS-466547 and**
466 **parent nuc GS-441524**

467 RDV-containing diastereometric mixture GS-466547 and parent nuc GS-441524 were tested at
468 10 μM in a SafetyScreen87 Panel (Eurofins Panlabs Taiwan, Ltd) (Table S3). Effects of

469 compounds were evaluated along with a known receptor ligand or substrate. Positive results were
470 defined as > 50% inhibition of ligand binding.

471 **Determination of GS-441524 and its Phosphorylated Metabolites in PC-3 and PHH.**

472 HEp-2, PC-3, or PHH cells were seeded 0.44×10^6 or 0.88×10^6 cells/well in 12-well plate
473 respectively. On the next day, HEp-2, PC-3, or PHH were treated with either 1 μM RDV or GS-
474 441524, in duplicate, or 0.01% DMSO in eight replicates. After 24 hours treatment, cells were
475 washed twice with ice-cold 0.9% NaCl then treated with 500 μL of dry ice-cold extraction buffer
476 (0.1% potassium hydroxide and 67 mM ethylenediamine tetraacetic acid in 70% methanol,
477 containing 0.5 μM chloro-adenosine triphosphate as internal standard). The above solution was
478 vortexed for 5 minutes, then centrifuged at 20,000 x g for 10 minutes. Supernatant was
479 transferred to clean 1.5 mL Eppendorf vials and loaded onto a centrifuging evaporator. Once
480 dry, samples were reconstituted with 80 μL of 1 mM ammonium phosphate buffer (pH 7.0), and
481 transferred to HPLC vials where a 10 μL injection was used for analysis by LC/MS/MS.
482 Standard calibration curves for HEp-2, PC-3, or PHH were constructed based on pmol of
483 compound per sample with known cell numbers in each sample. The standard curve was
484 prepared by spiking an appropriate amount of GS-441524, GS-441524-MP, GS-441524-DP, and
485 GS-443902 solution, prepared in water, into blank HEp-2, PC-3, or PHH matrix, with serial
486 dilution to complete the calibration standard curve. Detailed HPLC and mass spectrometry
487 parameters are provided in the Materials and Methods under Supplemental Materials.

488 **Determination of cell volume**

489 Measurements of the cell volume for various cell types were conducted using confocal
490 microscope Leica SP8 (Leica Microsystems GmbH, Wetzlar, Germany) and image analysis
491 software Imaris (Bitplane, Zürich, Switzerland). The intracellular space was labeled with a

492 fluorescent dye Calcein AM (1-10 $\mu\text{g}/\text{mL}$, ThermoFisher Scientific, Waltham, MA, USA),
493 which loads into live cells with active esterases. The nuclei were labeled with DNA-binding dye
494 Hoechst 33342 (16-32 μM , ThermoFisher Scientific, Waltham, MA, USA) to facilitate
495 separation and correct counting of adjacent cells. The labeling was conducted by incubating the
496 cells in a culture medium containing the dyes at 37 °C and 5% CO_2 for at least 15 min. The
497 series of images (Z-stacks) were collected using 63x objective with numerical aperture of 1.4 at
498 different focal planes to enable computational reconstruction of three-dimensional objects with
499 complex shape and estimation of their volume. Calcein was excited with the white laser at 488
500 nm and the fluorescence signal was detected in the range of 498-600 nm using Leica HyD hybrid
501 detector. The imaging was performed at 37 °C to avoid temperature-related changes in shape of
502 the cells. The estimation of the cell volume was verified using the fluorescent beads of known
503 diameter by comparison of the values obtained after calculations based on either the diameter or
504 3-D reconstruction. This revealed that only minor correction was needed to account for
505 elongation of the point spread function in vertical direction for the objective with high (1.4)
506 numerical aperture unlike for the objective with low (0.4) numerical aperture. In addition, the
507 results of confocal imaging were confirmed using the cell counter (Cellometer K2, Nexcelom
508 Bioscience, Lawrence, MA, USA) with imaging capabilities allowing for determining the
509 diameter of the cells in suspension after trypsinization.

510 **Statistical Analysis**

511 The difference between compound-treated groups and DMSO-treated group were analyzed using
512 ordinary one-way ANOVA (Sidak's multiple comparisons test) (GraphPad Prism 8.1) and a *p*-
513 values less than 0.05 was defined as stastically significant.

514

515 **Figures and legends**

516 Figure 1: Structures of RDV and major metabolites.

517 Figure 2: Effect of RDV on cellular ROS, ATP, and cell count after 24-hours of treatment in
518 HepG2 cells. (A) Treatment of 3.1-50 μM of RDV showed no effect on ROS, while 100 μM of
519 RDV caused a 60% increase in ROS ($p = 0.042$). The positive control menadione showed > 3-
520 fold increase in ROS levels after a 30-min incubation. (B) A concentration-dependent
521 cytotoxicity was observed during the 24-hour incubation of RDV, especially for concentrations \geq
522 12.5 μM .

523 Figure 3: Effects of RDV and its parent nucleoside GS-441524 on mitochondrial protein
524 synthesis after 5-days of treatment in PC-3 cells. The effects on COX-1 levels (● blue, solid
525 lines), SDH-A (◆ green, solid lines), and ATP levels (■ red, solid lines) are shown as % of
526 DMSO control. RDV showed non-selective inhibition of COX-1, SDH-A, and ATP levels while
527 GS-441524 showed no effect up to 100 μM . The positive control chloramphenicol, a known
528 mitochondrial toxin, specifically inhibited COX-1 synthesis.

529 Figure 4: Effect of RDV on mitochondrial respiration (spare respiratory capacity) (● blue, solid
530 lines), ATP levels (■ red, solid lines), and total DNA (◆ green, solid lines) after a 3-day
531 treatment in PC-3, HepG2, PHH, and RPTEC. The spare respiratory capacity was normalized by
532 cell numbers. Overall, RDV showed simultaneous inhibition of mitochondrial respiration, ATP
533 levels, and total DNA, except in PC-3 cells where a mitochondria-specific inhibition was
534 observed.

535 Figure 5. Metabolism of RDV and GS-441524 in HEp-2, PC-3, and PHH cells. The active 5'-
536 triphosphate levels were measured after 24-hr continuous incubation of each compound. RDV-

537 treated cells (open bars) formed 7.8-, 23-, and 23-fold higher triphosphate levels than GS-
538 441524-treated (filled bars) in HEP-2, PC-3, and PHH cells, respectively.

539

540

541 **Tables**

542 **Table 1: *In vitro* cytotoxicity of RDV and GS-441524 in human cell lines and primary**

543 **human cells after 5-14 day treatment**

Cells		CC ₅₀ (μM) ^{a,b}		
		RDV (SI) ^c	GS-441524	Positive Control ^d
Cell lines	HEp-2	6.0 ± 1.5 (600)	> 100	0.53 ± 0.10
	HepG2	3.7 ± 0.2 (370)	> 100	0.73 ± 0.01
	PC-3	8.9 ± 1.6 (890)	> 100	0.52 ± 0.11
	MT-4	1.7 ± 0.4 (170)	69 ± 26	0.12 ± 0.03
Primary cells	PHH	2.5 ± 0.6 (250)	> 100	1.60 ± 0.01
	RPTEC	12.9 ± 6.2 (12,900)	> 100	0.85 ± 0.01
	Quiescent PBMC	> 20 (>20,000)	> 100	5.05 ± 0.01
	Stimulated PBMC	14.8 ± 5.8 (14,800)	> 100	1.10 ± 0.01
	Erythroid progenitors	8.5 ± 1.9 (850)	13.9 ± 1.3	3.2 ± 1.6
	Myeloid progenitors	5.1 ± 2.3 (510)	11.7 ± 9.6 ^e	2.2 ± 0.6
	Megakaryoid progenitors	4.9 ± 2.5 (490)	9.6 ± 2.4	2.3 ± 1.7

544 ^a All CC₅₀ values represent the average ± SD of three or more independent experiments. Cells
 545 from three different donors were tested in the primary cell assays. The compounds were
 546 refreshed every other day during the 5-day PHH study.

547 ^b Treatment duration: all studies are 5 days except studies for the three human hematopoietic
 548 progenitor cells where a 11- to 14-day treatment was used.

549 ^c Selectivity Index (SI) = CC₅₀/EC₅₀, where the an EC₅₀ value of 10 nM against SARS-CoV-2
 550 was used (18).

551 ^d Positive control: puromycin was used in all assays except the three human hematopoietic
 552 progenitor cells where 5-fluorouracil was used as a positive control. CC₅₀ values of control
 553 compounds are consistent with historical values.

554 ^e The myeloid CC₅₀ values for GS-441524 tested against cells from three different donors were
 555 6.37, 22.70, and 5.93 μM, respectively.

556 **Table 2: *In vitro* cytotoxicity of RDV and GS-441524 under anaerobic and aerobic**
 557 **metabolic conditions after 5-day treatment in HepG2 and PC-3 cells**

Compound	5-day CC ₅₀ (μM) ^a			
	HepG2 Cells		PC-3 Cells	
	Anaerobic (Glucose)	Aerobic (Galactose)	Anaerobic (Glucose)	Aerobic (Galactose)
RDV	3.7 ± 0.2	11.1 ± 1.2	8.9 ± 1.6	1.4 ± 0.1
GS-441524	> 100	> 100	> 100	> 100
Puromycin	0.73 ± 0.01	0.96 ± 0.13	0.52 ± 0.11	0.48 ± 0.01

558 ^a All CC₅₀ values represent average ± SD of three or more independent experiments.

559

560 **Table 3: *In vitro* effect of RDV and GS-441524 on mitochondrial proteosynthesis after 5-**
 561 **day treatment in PC-3**

Compounds	Mitochondrial and Cellular Protein Synthesis 5-day CC ₅₀ (μM) ^a		
	COX-1	SDH-A	Cellular ATP
RDV	8.9 ± 1.1	8.6 ± 1.3	11.3 ± 3.3
GS-441524	> 100	> 100	> 100
Chloramphenicol (positive control)	2.6 ± 0.6	> 25	14.1 ± 3.6

562 ^a CC₅₀ values represent average ± SD of three or more independent experiments.

563

564

565 **Table 4: *In vitro* effect of RDV and its metabolites GS-704277 and GS-441524 on**
 566 **mitochondrial respiration after 3-day treatment in PC-3, HepG2, PHH, and RPTECs**

567

Compounds	Cell Model	3-day CC ₅₀ (μM) ^a		
		Spare Respiration	Total DNA Content	Cellular ATP
RDV	PC-3	2.5 ± 0.1	12.5 ± 0.7	24.0 ± 1.4
	HepG2	10.6 ± 0.1	6.3 ± 0.9	7.9 ± 0.1
	PHH	7.6 ± 1.9	13.4 ± 1.7	7.8 ± 2.2
	RPTECs	7.3 ± 2.7	14.3 ± 3.3	16.9 ± 4.1
GS-441524	PC-3	> 100	> 100	> 100
	HepG2	> 100	> 100	> 100
	PHH	> 100	> 100	> 100
	RPTECs	> 100	> 100	> 100
GS-704277	PHH	> 100	> 100	> 100
Control chloramphenical	PC-3	4.8 ± 1.3	> 50	> 50
Control phenformin	PHH	1.9 ± 0.5	22.1 ± 1.9	9.7 ± 4.5

568 ^a CC₅₀ values represent average ± SD from three or more independent experiments.

569

570

571

572 **Table 5: Inhibition of host DNA and RNA polymerases by the active triphosphate**
 573 **metabolite GS-443902**

Compound	IC ₅₀ (μM) ^a				
	DNA Pol α	DNA Pol β	DNA Pol γ	RNA Pol II	POLRMT Pol
GS-443902	> 200	> 200	> 200	> 200	> 200
Positive Control	Aphidicolin 4.7 ± 3.3	3'dTTP 1.9 ± 0.8	3'dTTP 1.2 ± 0.6	α-amanitin 0.0035 ± 0.0015	3'deoxy GTP 4.2 ± 1.4

574 ^a IC₅₀ values represent average ± SD from three independent experiments.

575

576

577

578 **Table 6: Relative rate of incorporation of the active triphosphate metabolite GS-443902 by**
 579 **human mitochondrial DNA and RNA polymerases**

Clinical Compounds	Nucleotide Triphosphate	Rate of Incorporation (% of natural dNTP or NTP) ^a	
		DNA Polymerase γ	mtRNA Polymerase
RDV	GS-443902	0%	5.8% ± 1.4%
Decitabine	5-aza-2'-dCTP	79% ± 8%	ND
BMS-986094	2'CMε-GTP	ND	92% ± 33%
Balapiravir/RG1626	4'CN-CTP	ND	112% ± 10%

580 ^a The rate of single nucleotide incorporation was measured in the presence of 50 μM nucleotide
 581 analog for DNA Pol γ and 500 μM for POLRMT and expressed as % of the natural dNTP or
 582 NTP incorporation at the same concentration. Data are presented as average ± SD from three or
 583 more independent experiments.

584

585 **ACKNOWLEDGMENTS**

586 Becky Norquist provided medical writing assistance on behalf of Gilead. All authors are
587 employees of Gilead Sciences, Inc. except O.B. and M.P. who were previously employed by
588 Gilead Sciences, Inc. All authors may hold stock or stock options in Gilead Sciences, Inc.

589 **FUNDING INFORMATION**

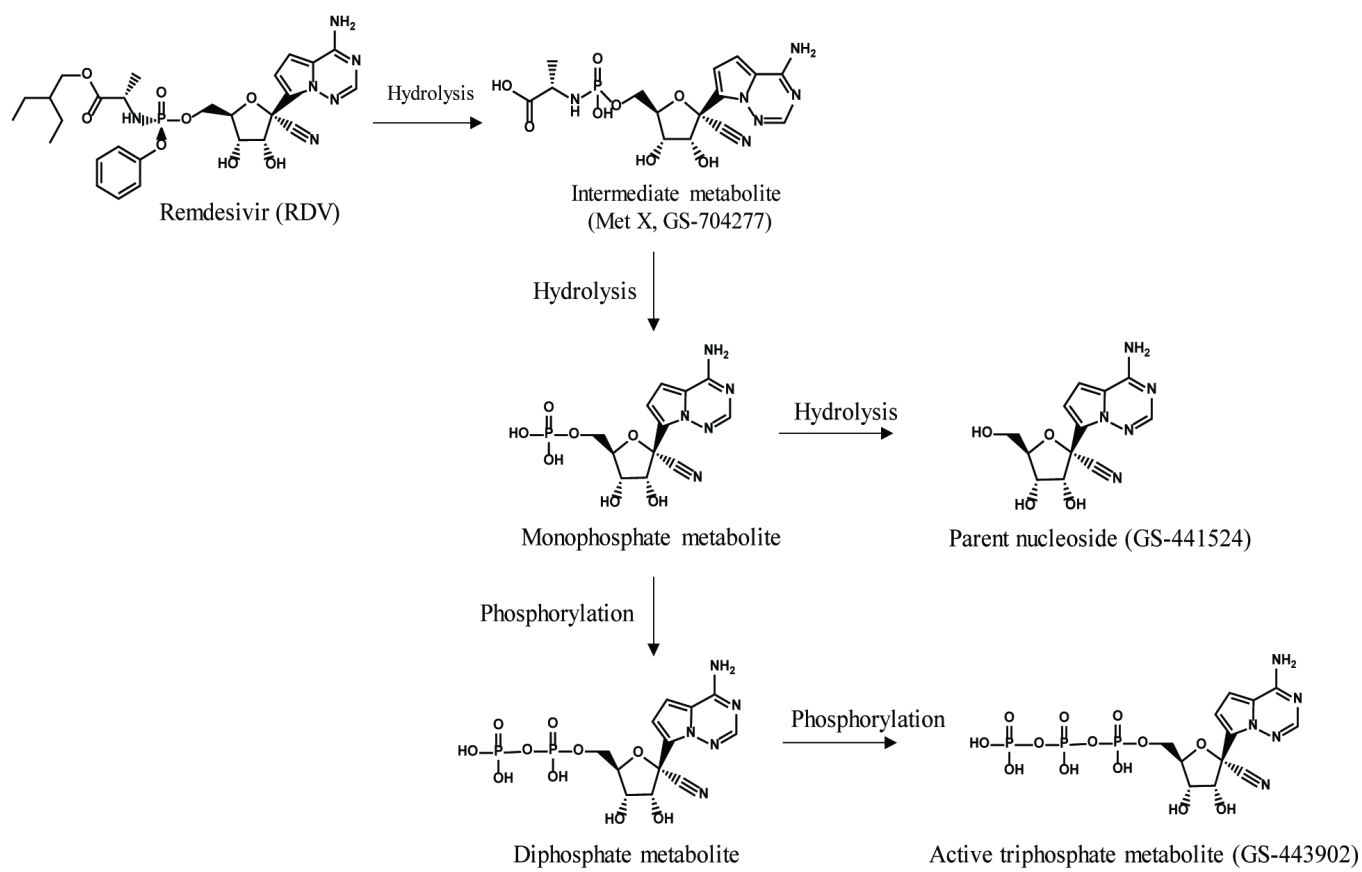
590 The studies were fully sponsored by Gilead Sciences, Inc.

591 **References**

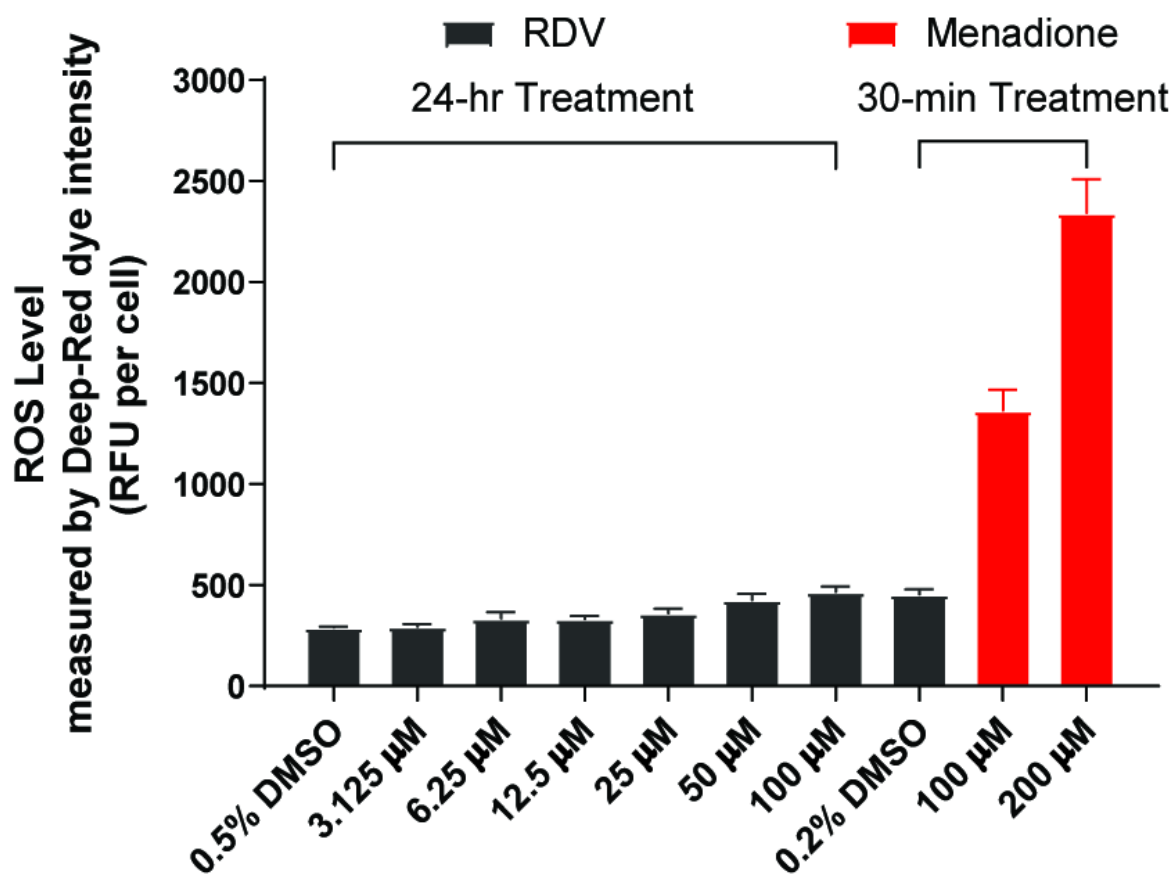
- 592 1. De Clercq E. 2011. A 40-year journey in search of selective antiviral chemotherapy. *Annu Rev*
593 *Pharmacol Toxicol* 51:1-24.
- 594 2. Asselah T, Marcellin P, Schinazi RF. 2018. Treatment of hepatitis C virus infection with direct-
595 acting antiviral agents: 100% cure? *Liver Int* 38 Suppl 1:7-13.
- 596 3. Johnson AA, Ray AS, Hanes J, Suo Z, Colacino JM, Anderson KS, Johnson KA. 2001. Toxicity of
597 antiviral nucleoside analogs and the human mitochondrial DNA polymerase. *Journal of Biological*
598 *Chemistry* 276:40847-40857.
- 599 4. Arnold JJ, Sharma SD, Feng JY, Ray AS, Smidansky ED, Kireeva ML, Cho A, Perry J, Vela JE, Park Y,
600 Xu Y, Tian Y, Babusis D, Barauskas O, Peterson BR, Gnatt A, Kashlev M, Zhong W, Cameron CE.
601 2012. Sensitivity of Mitochondrial Transcription and Resistance of RNA Polymerase II Dependent
602 Nuclear Transcription to Antiviral Ribonucleosides. *PLoS Pathog* 8:e1003030.
- 603 5. Feng JY, Xu Y, Barauskas O, Perry JK, Ahmadyar S, Stepan G, Yu H, Babusis D, Park Y, McCutcheon
604 K, Perron M, Schultz BE, Sakowicz R, Ray AS. 2016. Role of Mitochondrial RNA Polymerase in the
605 Toxicity of Nucleotide Inhibitors of Hepatitis C Virus. *Antimicrob Agents Chemother* 60:806-17.
- 606 6. Feng JY. 2018. Addressing the Selectivity and Toxicity of Antiviral Nucleosides. *Antivir Chem*
607 *Chemother* 26:1-8.
- 608 7. Sheahan TP, Sims AC, Graham RL, Menachery VD, Gralinski LE, Case JB, Leist SR, Pirc K, Feng JY,
609 Trantcheva I, Bannister R, Park Y, Babusis D, Clarke MO, Mackman RL, Spahn JE, Palmiotti CA,
610 Siegel D, Ray AS, Cihlar T, Jordan R, Denison MR, Baric RS. 2017. Broad-Spectrum Antiviral GS-
611 5734 Inhibits Both Epidemic and Zoonotic Coronaviruses. *Sci Transl Med* 9:eaal3653.
- 612 8. Sheahan TP, Sims AC, Leist SR, Schafer A, Won J, Brown AJ, Montgomery SA, Hogg A, Babusis D,
613 Clarke MO, Spahn JE, Bauer L, Sellers S, Porter D, Feng JY, Cihlar T, Jordan R, Denison MR, Baric
614 RS. 2020. Comparative Therapeutic Efficacy of Remdesivir and Combination Lopinavir, Ritonavir,
615 and Interferon Beta Against MERS-CoV. *Nat Commun* 11:222.
- 616 9. Porter DP, Weidner JM, Gomba L, Bannister R, Blair C, Jordan R, Wells J, Wetzel K, Garza N, Van
617 Tongeren S, Donnelly G, Steffens J, Moreau A, Bearss J, Lee E, Bavari S, Cihlar T, Warren TK.
618 2020. Remdesivir (GS-5734) is Efficacious in Cynomolgus Macaques Infected with Marburg Virus.
619 *J Infect Dis* doi:10.1093/infdis/jiaa290:1-8.
- 620 10. Warren TK, Jordan R, Lo MK, Ray AS, Mackman RL, Soloveva V, Siegel D, Perron M, Bannister R,
621 Hui HC, Larson N, Strickley R, Wells J, Stuthman KS, Van Tongeren SA, Garza NL, Donnelly G,
622 Shurtleff AC, Retterer CJ, Gharaibeh D, Zamani R, Kenny T, Eaton BP, Grimes E, Welch LS, Gomba
623 L, Wilhelmson CL, Nichols DK, Nuss JE, Nagle ER, Kugelman JR, Palacios G, Doerffler E, Neville S,
624 Carra E, Clarke MO, Zhang L, Lew W, Ross B, Wang Q, Chun K, Wolfe L, Babusis D, Park Y, Stray
625 KM, Trancheva I, Feng JY, Barauskas O, Xu Y, Wong P, et al. 2016. Therapeutic efficacy of the
626 small molecule GS-5734 against Ebola virus in rhesus monkeys. *Nature* 531:381-5.
- 627 11. Jordan PC, Liu C, Raynaud P, Lo MK, Spiropoulou CF, Symons JA, Beigelman L, Deval J. 2018.
628 Initiation, Extension, and Termination of RNA Synthesis by a Paramyxovirus Polymerase. *PLoS*
629 *Pathog* 14:e1006889.
- 630 12. Lo MK, Feldmann F, Gary JM, Jordan R, Bannister R, Cronin J, Patel NR, Klens JD, Nichol ST, Cihlar
631 T, Zaki SR, Feldmann H, Spiropoulou CF, de Wit E. 2019. Remdesivir (GS-5734) protects African
632 green monkeys from Nipah virus challenge. *Sci Transl Med* 11:eaau9242.
- 633 13. Humeniuk R, Mathias A, Cao H, Osinusi A, Shen G, Chng E, Ling J, Vu A, German P. 2020. Safety,
634 Tolerability, and Pharmacokinetics of Remdesivir, An Antiviral for Treatment of COVID-19, in
635 Healthy Subjects. *Clin Transl Sci* 13:896-906.
- 636 14. Mulangu S, Dodd LE, Davey RT, Jr., Tshiani Mbaya O, Proschan M, Mukadi D, Lusakibanza Manzo
637 M, Nzolo D, Tshomba Oloma A, Ibanda A, Ali R, Coulibaly S, Levine AC, Grais R, Diaz J, Lane HC,

- 638 Muyembe-Tamfum JJ, Group PW, Sivahera B, Camara M, Kojan R, Walker R, Digheo-Kemp B,
639 Cao H, Mukumbayi P, Mbala-Kingebeni P, Ahuka S, Albert S, Bonnett T, Crozier I, Duvenhage M,
640 Proffitt C, Teitelbaum M, Moench T, Aboulhab J, Barrett K, Cahill K, Cone K, Eckes R, Hensley L,
641 Herpin B, Higgs E, Ledgerwood J, Pierson J, Smolskis M, Sow Y, Tierney J, Sivapalasingam S,
642 Holman W, Gettinger N, et al. 2019. A Randomized, Controlled Trial of Ebola Virus Disease
643 Therapeutics. *N Engl J Med* 381:2293-303.
- 644 15. Goldman JD, Lye DCB, Hui DS, Marks KM, Bruno R, Montejano R, Spinner CD, Galli M, Ahn MY,
645 Nahass RG, Chen YS, SenGupta D, Hyland RH, Phil D, Osinusi AO, Cao H, Blair C, Wei X, Gaggar A,
646 Brainard DM, Towner WJ, Munoz J, Mullane KM, Marty FM, Tashima KT, Diaz G, Subramanian A.
647 2020. Remdesivir for 5 or 10 Days in Patients with Severe Covid-19. *N Engl J Med*:1-11.
- 648 16. Beigel JH, Tomashek KM, Dodd LE, Mehta AK, Zingman BS, Kalil AC, Hohmann E, Chu HY,
649 Luetkemeyer A, Kline S, Lopez de Castilla D, Finberg RW, Dierberg K, Tapson V, Hsieh L,
650 Patterson TF, Paredes R, Sweeney DA, Short WR, Touloumi G, Lye DC, Ohmagari N, Oh M, Ruiz-
651 Palacios GM, Benfield T, Fatkenheuer G, Kortepeter MG, Atmar RL, Creech CB, Lundgren J,
652 Babiker AG, Pett S, Neaton JD, Burgess TH, Bonnett T, Green M, Makowski M, Osinusi A, Nayak
653 S, Lane HC. 2020. Remdesivir for the Treatment of Covid-19 — Final Report. *N Engl J Med*.
- 654 17. Spinner CD, Gottlieb RL, Criner GJ, Arribas Lopez JR, Cattelan AM, Soriano Viladomiu A, Ogbuagu
655 O, Malhotra P, Mullane KM, Castagna A, Chai LYA, Roestenberg M, Tsang OTY, Bernasconi E, Le
656 Turnier P, Chang SC, SenGupta D, Hyland RH, Osinusi AO, Cao H, Blair C, Wang H, Gaggar A,
657 Brainard DM, McPhail MJ, Bhagani S, Ahn MY, Sanyal AJ, Huhn G, Marty FM, Investigators G-U-
658 2020. Effect of Remdesivir vs Standard Care on Clinical Status at 11 Days in Patients With
659 Moderate COVID-19: A Randomized Clinical Trial. *JAMA* 324:1048-1057.
- 660 18. Pruijssers AJ, George AS, Schafer A, Leist SR, Gralinski LE, Dinnon KH, 3rd, Yount BL, Agostini ML,
661 Stevens LJ, Chappell JD, Lu X, Hughes TM, Gully K, Martinez DR, Brown AJ, Graham RL, Perry JK,
662 Du Pont V, Pitts J, Ma B, Babusis D, Murakami E, Feng JY, Bilello JP, Porter DP, Cihlar T, Baric RS,
663 Denison MR, Sheahan TP. 2020. Remdesivir Inhibits SARS-CoV-2 in Human Lung Cells and
664 Chimeric SARS-CoV Expressing the SARS-CoV-2 RNA Polymerase in Mice. *Cell Reports* 32:107940.
- 665 19. Feng JY, Cheng G, Perry J, Barauskas O, Xu Y, Fenaux M, Eng S, Tirunagari N, Peng B, Yu M, Tian
666 Y, Lee YJ, Stepan G, Lagpacan LL, Jin D, Hung M, Ku KS, Han B, Kitrinis K, Perron M, Birkus G,
667 Wong KA, Zhong W, Kim CU, Carey A, Cho A, Ray AS. 2014. Inhibition of Hepatitis C Virus
668 Replication by GS-6620, a Potent C-Nucleoside Monophosphate Prodrug. *Antimicrob Agents*
669 *Chemother* 58:1930-42.
- 670 20. Shuhendler AJ, Pu K, Cui L, Uetrecht JP, Rao J. 2014. Real-Time Imaging of Oxidative and
671 Nitrosative Stress in the Liver of Live Animals for Drug-Toxicity Testing. *Nat Biotechnol* 32:373-
672 80.
- 673 21. Marroquin LD, Hynes J, Dykens JA, Jamieson JD, Will Y. 2007. Circumventing the Crabtree effect:
674 replacing media glucose with galactose increases susceptibility of HepG2 cells to mitochondrial
675 toxicants. *Toxicol Sci* 97:539-47.
- 676 22. Beeson CC, Beeson GC, Schnellmann RG. 2010. A high-throughput respirometric assay for
677 mitochondrial biogenesis and toxicity. *Anal Biochem* 404:75-81.
- 678 23. Nadanaciva S, Rana P, Beeson GC, Chen D, Ferrick DA, Beeson CC, Will Y. 2012. Assessment of
679 drug-induced mitochondrial dysfunction via altered cellular respiration and acidification
680 measured in a 96-well platform. *J Bioenerg Biomembr* 44:421-37.
- 681 24. Dranka BP, Benavides GA, Diers AR, Giordano S, Zelickson BR, Reily C, Zou L, Chatham JC, Hill BG,
682 Zhang J, Landar A, Darley-Usmar VM. 2011. Assessing bioenergetic function in response to
683 oxidative stress by metabolic profiling. *Free Radic Biol Med* 51:1621-35.

- 684 25. Zhang C, Shi L, Wang FS. 2020. Liver Injury in COVID-19: Management and Challenges. *Lancet*
685 *Gastroenterol Hepatol* 5.
- 686 26. Pessina A, Albella B, Bayo M, Bueren J, Brantom P, Casati S, Croera C, Gagliardi G, Foti P,
687 Parchment R, Parent-Massin D, Schoeters G, Sibiril Y, Van Den Heuvel R, Gribaldo L. 2003.
688 Application of the CFU-GM Assay to Predict Acute Drug-Induced Neutropenia: An International
689 Blind Trial to Validate a Prediction Model for the Maximum Tolerated Dose (MTD) of
690 Myelosuppressive Xenobiotics. *Toxicological Sciences* 75:355-367.
- 691 27. Livak KJ, Schmittgen TD. 2001. Analysis of relative gene expression data using real-time
692 quantitative PCR and the 2(-Delta Delta C(T)) Method. *Methods* 25:402-8.
- 693 28. Birkus G, Hitchcock MJM, Cihlar T. 2002. Assessment of mitochondrial toxicity in human cells
694 treated with tenofovir: comparison with other nucleoside reverse transcriptase inhibitors.
695 *Antimicrobial Agents and Chemotherapy* 46:716-723.
- 696 29. Clarke MO, Mackman R, Byun D, Hui H, Barauskas O, Birkus G, Chun BK, Doerffler E, Feng J, Karki
697 K, Lee G, Perron M, Siegel D, Swaminathan S, Lee W. 2015. Discovery of beta-d-2'-deoxy-2'-
698 alpha-fluoro-4'-alpha-cyano-5-aza-7,9-dideaza adenosine as a potent nucleoside inhibitor of
699 respiratory syncytial virus with excellent selectivity over mitochondrial RNA and DNA
700 polymerases. *Bioorg Med Chem Lett* doi:10.1016/j.bmcl.2015.04.073.
- 701 30. Smidansky ED, Arnold JJ, Reynolds SL, Cameron CE. 2011. Human Mitochondrial RNA
702 Polymerase: Evaluation of the Single-Nucleotide-Addition Cycle on Synthetic RNA/DNA
703 Scaffolds. *Biochemistry* 50:5016-32.
- 704 31. Akinci E, Cha M, Lin L, Yeo G, Hamilton CM, Donahue JC, Bermudez-Cabrera CH, Zanetti CL, Chen
705 M, Barkal AS, Khowpinitchai B, Chu N, Velimirovic M, Jodhani R, Fife DJ, Sovrovic M, Cole AP,
706 Davey AR, Cassa AC, Sherwood IR. 2020. Elucidation of remdesivir cytotoxicity pathways through
707 genome-wide CRISPR-Cas9 screening and transcriptomics. *BioRxiv preprint* doi:
708 <https://doi.org/10.1101/2020.08.27.270819>.
- 709



A



B

